ORIGINAL RESEARCH ARTICLE

Effect of Cryogenic Cooling on Micro-milling Properties of Titanium Alloy

Fengbiao Wang, Qiusheng Pang, Qi Yang, and Hui Han

Due to the micro-burrs and size effect often associated with titanium alloy micro-milling, the cutting quality is inevitably influenced. This paper presents the first comprehensive investigation on the machining properties of micro-milling titanium alloy at cryogenic cooling. Based on the strain gradient plasticity theory, the minimum milling thickness model was established considering scale effect, and the minimum milling thickness was simulated and deduced. Compared with conventional dry (20 °C) and cryogenic cooling ($-$ 190 °C) milling, a series of micro-milling experiments were carried out, which was included in the milling parameters such as v_c = 40 m/min, a_p = 20-50 μm, f_z = 1-2.5 μm/r, a_e = 1 mm, and so on. The results show that the processed groove surface is smooth compared to conventional milling, and the burr is hardly visible and followed high chips breaking rate at cryogenic cooling, and the surface roughness value is obviously decreased. Besides, in the range of f_z = 1-2.5 μm/z, the main milling force decreases first and then increases. A scale effect is generated at f_z = 1.5 μm with the smallest milling force. At LN$_2$ cryogenic cooling micro-milling strategy, the improved machining properties, tool life and processing efficiency can be obtained with a larger per tooth feed and lower depth of cut.

1. Introduction

The application level of advanced materials represented by titanium alloy has become the important indicators for the high-end equipment. Meanwhile, the titanium alloy microstructural components are indispensable, such as the lunar rover bearing parts, missile-shaped inlet parts, micro-aircraft blades, and so on. Titanium alloy has the lower thermal conductivity (14 W/(m K), only 15-20% of 45 steel) and elastic modulus (107 GPa, about 1/2 of 45 steel), high temperature chemical affinity. These characteristics had led to high cutting temperature, easy tool wear, and strong material adhesion in the conventional micro-cutting process (Ref 1, 2). Therefore, the micro-machining accuracy was commonly poor as well as the only about 25% processing efficiency (Ref 3, 4).

In micro-milling of titanium alloy, it is difficult to control and remove burrs both during and after processing. Because of the small feature scale of micro-parts, the relative size of burr was much larger than that of conventional milling. So, the conventional deburring method was difficult to apply to these tiny parts (Ref 5, 6). The formation of burrs would directly affect the surface processing quality of micro-parts. Meanwhile, the feature size of micro-machining parts was smaller as well as

the unstable cutting force. It is difficult to obtain the way to remove micro-burrs by changing the tool geometric and process parameters. And the surface quality was difficult to be controlled, which had a great impact on the normal work of high-precision workpiece.

To solve the problem of micro-machining of titanium alloy, some researchers had made a lot of exploration and beneficial attempts, including optimizing machining parameters and seeking new processing methods. Aslantas et al. (Ref 7) adopted response surface method to carry out multi-objective optimization of micro-turning Ti-6Al-4V alloy process parameters such as cutting speed, feed speed and cutting depth. The results showed that feed speed was an important factor affecting the response of micro-turning machining. Martin et al. (Ref 8) established a dynamic model of micro-end milling force and vibration and studied the unique chip formation mechanism and the dynamic characteristics. Bao and Tansel (Ref 9) proposed an improved cutting force model. The model considered the tool nose trajectory and calculated the change of chip thickness, and the experiment verifies the model was more accurate than the conventional model. Liu et al. (Ref 10) discussed the effects of the minimum cutting thickness, plastic deformation and the machined material characteristics on the chip formation and analyzed and pointed out that the micro-cutting machinability was affected by the machining thermal effect, dynamic characteristics, minimum cutting thickness and scale effect.

Lee et al. (Ref 11) studied the generated burrs during micro-milling titanium alloy through experiments. He reported the burr size was increased with the increase of the amount of depth of cut and feed. Schmidt et al. (Ref 12) found the height of burrs was commonly 5-60 μm, and the down-milling would have the larger burr. Fu (Ref 13) deeply analyzed the formation mechanism and influencing factors of burrs and pointed out the burr was increased with the increase of blunt radius of blade edge. Subbiah et al. (Ref 14) conducted extensive studies on the

Fengbiao Wang, Qiusheng Pang, Qi Yang, and Hui Han, School of Mechanical Engineering, Shenyang Ligong University, Shenyang 110159, China. Contact e-mail: yangqi197602@163.com.

additional energy required of the fracture and separation of workpiece materials, which was the main cause of scale effect. Kopalinsky (Ref 15) identified the cutting speed in micro-cutting was usually lower, and the reduction temperature resulted in the decrease of shear angle, which ultimately leaded to the scale effect.

In recent years, some scholars had found that the material properties and microstructure had significant changes at cryogenic temperature, which affected the material's machinability. Meanwhile, they had conducted some cryogenic cooling process for titanium alloys. Mozammel (Ref 16) studied the cutting force and surface roughness of processing titanium alloy by cryogenic and conventional cooling through full-factor test. They reported that the cryogenic cooling strategy was better than conventional one. Park et al. (Ref 17) adopted cryogenic cooling method to carry out the end milling for titanium alloy with greater depth of cut. That greatly reduced the milling force, and the service life of tool was increased by 32% compared with the conventional cooling. Shokrani et al. (Ref 18) contrasted milling performances of titanium alloy in three different cooling ways including dry cutting, cutting fluid and liquid nitrogen. They summarized that the surface roughness value was reduced by 30-40%, and the chemical reactions were effectively suppressed between tool and workpiece.

Some scholars have used low temperature cooling method for micro-machining. Kakinuma (Ref 19) used LN_2 freezing milling to process polydimethylsiloxane (PDMS) in micro-grooves and found that the hardness of the material increased at lower temperature, and it could be processed into micro-grooves with good processing accuracy. Aslantas (Ref 20) used chilled air to cool the micro-turning titanium alloy, and reported that the cutting force was increased by 80% and the surface roughness value was decreased. When drilling titanium alloy, chilled air cooling can reduce the burr height (Ref 21). In the process of micro-cutting Inconel 718 with cryogenic precooling, he also found that the roughness value and burr amount of machined surface were significantly all reduced (Ref 22).

This paper aims at the defects such as difficult chip breaking, high milling temperature gradient and serious burring in conventional micro-milling of titanium alloy. A micro-milling simulation model based on minimum milling thickness is established. Meanwhile, a series of contrast experiments including conventional and cryogenic cooling will be carried out. Furthermore, the machinability such as surface defects and surface roughness will be investigated and analyzed, and so on.

2. Micro-milling Model at Cryogenic

2.1 Mesoscale Micro-cutting Model

Micro-milling of Ti-6Al-4V is a complex machining process, which is accompanied by large elastic–plastic deformation, high strain and thermoviscoplasticity deformation at high temperature. Meanwhile, the scale effect based on strain gradient theory and dislocation theory is also needed to be reflected. So, the traditional J–C constitutive model relationship expression is as follows (Ref 23, 24).

$$\sigma_{JC} = (A + B\varepsilon^n)\left[1 + C\ln\left(\frac{\dot{\varepsilon}}{\dot{\varepsilon}_0}\right)\right]\left[1 - \left(\frac{T - T_0}{T_m - T_0}\right)^t\right] \quad (Eq\ 1)$$

where σ_{JC} is the stress (MPa), A is the material yield strength under quasi static, B is the influence coefficient of strain hardening, C is the strain rate sensitivity coefficient, n is strain rate sensitivity index, ε is the strain, $\dot{\varepsilon}$ is the equivalent plastic strain rate, $\dot{\varepsilon}_0$ is the reference strain rate, T is the deformation temperature (°C), T_0 is the reference temperature (°C), T_m is the material melting point (°C), and t is the thermal softening coefficient of material.

Considering the strain gradient plasticity theory of dislocation mechanism, the material constitutive relation is expressed as a function of dislocation density through Taylor equation (Ref 25).

$$\tau = \partial G_t b\sqrt{\rho} = \partial G_t b\sqrt{\rho_s + \rho_g} \quad (Eq\ 2)$$

where τ is the shear flow stress (MPa), ∂ is an empirical constant (between 0.2 and 0.5), G_t is the shear modulus (GPa), and it is 56.7 GPa at 20 °C and 63.2 GPa at − 196 °C, b is the Burgers vector, ρ is the total dislocation density, ρ_s is the statistical store dislocation, and ρ_g is the geometrically required dislocation.

The relationship between the geometrically necessary dislocation ρ_g and the strain gradient η is as follows.

$$\rho_g = \frac{2\eta}{b} \quad (Eq\ 3)$$

The statistical storage dislocation ρ_s is independent of strain gradient and can be determined by material experiments.

$$\sigma_c = 3\partial G_t b\sqrt{\rho_s} \quad (Eq\ 4)$$

The relationship between tensile stress σ and shear stress τ is as follows.

$$\sigma = 3\tau = 3\partial G_t b\sqrt{\rho_s + \rho_g} \quad (Eq\ 5)$$

In order to make the dislocation density at mesoscopic scale more accurate, the correction coefficient m is introduced, then Eq 6 can be expressed.

$$\sigma = 3\partial G_t b\sqrt{\rho_s^m + \rho_g^m} \quad (Eq\ 6)$$

Substitute Eq 3 and 4 into Eq 6 that can be obtained.

$$\sigma = \sigma_c\sqrt{1 + \left(\frac{18\partial^2 G_t^2 b\eta}{\sigma_c^2}\right)^m} \quad (Eq\ 7)$$

Let σ_{JC} replace σ_c such as $\sigma_c = \sigma_{JC}$, Eq 7 can be expressed as follows.

$$\sigma = \sigma_{JC}\sqrt{1 + \left(\frac{18\partial^2 G_t^2 b\eta}{\sigma_{JC}^2}\right)^m} \quad (Eq\ 8)$$

2.2 Plastic Strain Gradient in Shear Zone

Based on the strain gradient plasticity theory, Joshi et al. (Ref 26, 27) used the parallel shear zone model to represent the effective strain gradient in the principal shear zone. By analyzing the crystal dislocation in the principal shear zone as shown in Fig. 1, the relationship between the strain gradient η in the principal shear zone and the deformation length L can be obtained.
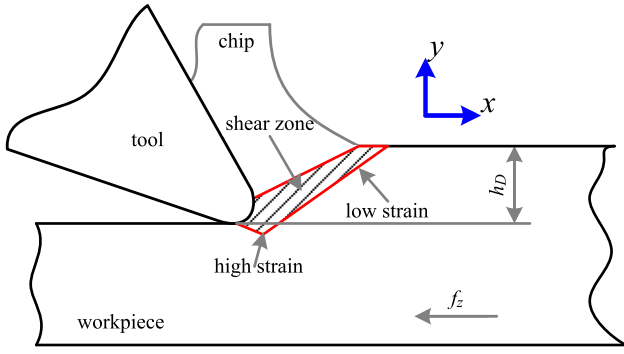
Fig. 1 Schematic representation of the main shear region at the mesoscopic scale

$$\eta = \frac{1}{L} \qquad \text{(Eq 9)}$$

By substituting Eq 9 into Eq 8, a material constitutive model considering plastic strain gradient at mesoscopic scale can be obtained.

$$\sigma = \sigma_{JC}\sqrt{1 + \left(\frac{18\partial^2 G_t^2 b}{\sigma_{JC}^2 \cdot L}\right)^m} \qquad \text{(Eq 10)}$$

And the key to the establishment of the constitutive model will be deduced by the solution of the length L of the shear zone

Due to the phenomenon of minimum cutting thickness involved in micro-machining, Lucca et al. (Ref 26) reported when the cutting thickness was close to the radius of the cutting edge of the tool, the circular radius would make the tool rake angle become effective negative rake angle and that would significantly increase the plowing force and cause scale effect. With the gradual increase of the cutting depth, it can be divided into three processing stages at the mesoscale:

1. When the cutting depth is far less than the tool nose blunt radius, the workpiece surface only generates elastic deformation.
2. When the cutting depth is close to the blunt radius, the cutting rake angle is a negative value, the plowing phenomenon is occurred, and the workpiece surface will generate elastic–plastic deformation.
3. When the cutting depth is further increased, the chips will be generated. This process leads to the generation of discontinuous chips, and it can also be deduced that there must be a minimum cutting thickness in the transition process from plow cutting to generating chips (Ref 29). So, the calculation of the minimum cutting thickness is very important, which will affect the precision and accuracy of micro-milling modeling.

Here, the cutting process can be divided into two situations: no chip formation and chip formation in Fig. 2.

When the actual m thickness h_D is less than the minimum $h_{D\min}$, as shown in Fig. 2(a), the elastoplastic deformation of material will be occurred under the extrusion of tool, and the material is mainly subjected to the plowing action without generating chips. In this case, the shear zone length L can be expressed.

$$L = \frac{\arccos\left(\frac{r_\varepsilon - h_D}{r_\varepsilon}\right)\pi r_\varepsilon}{180} \qquad \text{(Eq 11)}$$

where r_ε is the tool nose arc radius (μm), h_D is the milling thickness (μm).

As shown in Fig. 2(b), when the milling thickness is greater than the minimum milling thickness, the chips will be generated. According to the cutting theory, the length of the shear zone can be obtained.

$$L = \frac{h_D}{\sin\varphi} \qquad \text{(Eq 12)}$$

where φ is the shear angle (°).

$$\varphi = \arctan\frac{\cos\gamma}{\frac{a_c}{h_D} - \sin\gamma} \qquad \text{(Eq 13)}$$

where γ is the tool rake angle (°), a_c is the chip thickness (μm).

At cryogenic cooling, the brittleness of titanium alloy is increased as well as the elastic modulus, and the fracture elongation and the elastic deformation are decreased (Table 1). Similarly, it can easily be indicated from Eq 13 that the shear zone L also is decreased at cryogenic as well as the shear deformation. Furthermore, the workpiece material also is exhibited the brittle shear effect.

The equation for minimum milling thickness of titanium alloy can be derived from previous studies (Ref 34).

$$h_{D\min} = r_\varepsilon\left[1 - \cos\left(\frac{\pi}{4} - \frac{\beta}{2}\right)\right] = r_\varepsilon\left[1 - \cos\left(\frac{\pi}{4} - \frac{\arctan\mu}{2}\right)\right] \qquad \text{(Eq 14)}$$

where β is the friction angle between the tool and the material (°), μ is the friction coefficient between the tool and the workpiece.

As can be illuminated from Eq 14, the minimum milling thickness $h_{D\min}$ is obviously related to not only the tool nose arc radius r_ε, but also the friction coefficient μ between tool and workpiece in milling area. In addition, due to the change of material properties, the friction coefficient of the tool/workpiece interface is affected with the change of temperature. Based on the friction perspective, the thermal effect and dynamic characteristics were the two main factors which lead to friction generation and energy consumption (Ref 35). Gong et al. (Ref 36) established a calculation model of sliding friction coefficient based on the thermodynamic coupling process of friction interface.

$$\mu_T = \frac{4S^2 \cdot v_m^2 \cdot H^2}{P_T \cdot a \cdot m\left(a^2 \cdot \varpi_n^2 - 4\kappa^2 v_m^2\right)^2} \qquad \text{(Eq 15)}$$

where S is the actual contact area, v_m is relative speed of friction pair (m/min), namely cutting speed v_c, H is excitation force amplitude N, P_T is the normal load of friction pair, namely positive pressure F_y, a is lattice constant, and m is average atomic mass. For tool materials, ω_n is the angular frequency of lattice vibration rad/s, and κ is elastic force constant of crystal.

$$\mu_T = \frac{4S^2 \cdot v_c^2 \cdot H^2}{F_y \cdot a \cdot m\left(a^2 \cdot \varpi_n^2 - 4\kappa^2 v_c^2\right)^2} \qquad \text{(Eq 16)}$$
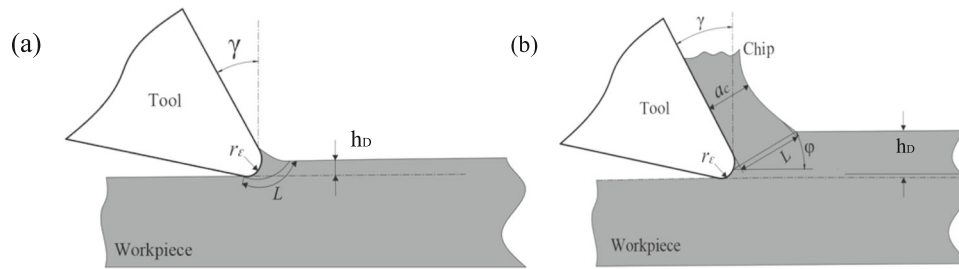
Fig. 2 Microchip formation. (a) No formed chip (b) Formed chip

Table 1 Mechanical properties of Ti-6Al-4V (Ref 30-33)

Temperature, °C	Yield strength, MPa	Tensile strength, MPa	Elasticity modulus, GPa	Shear strength, GPa	Elongation, %
20	890	960	107	56.7	14
− 30	1036	1077	113	57.1	…
− 78	1160	1100	120	59.5	13
− 150	1300	1225	…	…	11
− 196	1420	1500	133	63.2	10

Table 2 Parameters of micro-milling simulation

Milling speed v_c, m/min	Depth of cut a_p, μm	Feed f_z, μm/r	Radial depth of cut a_e, mm	Cooling temperature T, °C	Edge radius, mm
40	1	1		20	0.005
	1.25	1.25	1		
	1.5	1.5		LN$_2$ − 190	

It can be deduced from the above equation that the decreased temperature will lead to the increased elastic modulus as well as the cutting force, which will result in the increase of the normal load P_T. Furthermore, P_T will result in the decrease of friction coefficient and finally the increase of the minimum milling thickness.

2.3 Minimum Milling Thickness

The minimum milling thickness $h_{D\min}$ in the process of micro-milling is mainly reflected in the minimum cutting depth and the minimum feed per tooth. The minimum milling thickness can be studied by changing different cutting depths and feed rate. In simulation model, the milling parameters include v_c = 40 m/min, a_p = 1-2.5 μm/r, f_z = 1-2.5 μm/r, a_e = 1 mm, and so on (Table 2).

Due to the different mechanical properties of materials at room temperature 20 °C and cryogenic − 190 °C, the chip breaking characteristic is different. As shown in Fig. 3 and 4, compared with conventional dry cutting, the chip is long strip, but short block chip at cryogenic which is reflected as brittle chip breaking. Therefore, it can be inferred that the minimum milling thickness under the two cutting strategies is different and shall be comparative analysis.

The minimum milling thickness is directly determined by the radius of the cutting edge of the tool. In order to study the relationship between the minimum milling thickness and the radius of the cutting edge under the condition of cryogenic cooling, the cutting depth (corresponding to the feed per tooth of milling) is calculated by simulation analysis. Two-dimensional simulations were performed in $0.2r_\varepsilon$ (1 μm), $0.25r_\varepsilon$ (1.25 μm), and $0.3r_\varepsilon$ (1.5 μm) cases, and the results were shown in the figure.

In Fig. 5, when the milling thickness is $0.2r_\varepsilon$, the workpiece only generated elastic deformation under the extrusion of tool, and no chips are generated. When the milling thickness continues to be increased to $0.25r_\varepsilon$, the workpiece begins to generate elastic-plastic deformation, and the tool rake angle becomes negative, which results in material accumulation and local plastic deformation at the tool nose. When the milling thickness increases to $0.3r_\varepsilon$, the material begins to be separated and forms stable chips due to shearing. At the same time, the front knife of the tool is squeezed against the workpiece, resulting in plastic deformation of material, as well as the intensified bonding effect between tool and chip.

In Fig. 6, the removed effect of workpiece at cryogenic temperature is significantly less than conventional cutting during the overall cutting. The effect of LN$_2$ cryogenic impact will rapidly reduce the cutting zone temperature, and the bonding effect and friction coefficient are decreased. That is conducive to promoting the formation of chips and results in an increase of the minimum milling thickness. Furthermore, significant chips are generated at $0.3r_\varepsilon$ because of the accumulation of material on the rake face. So, the minimum milling thickness of a micro-tool with a 5 μm radius should be between $0.25r_\varepsilon$ (1.25 μm) and $0.3r_\varepsilon$ (1.5 μm) when milling titanium alloy at cryogenic cooling.
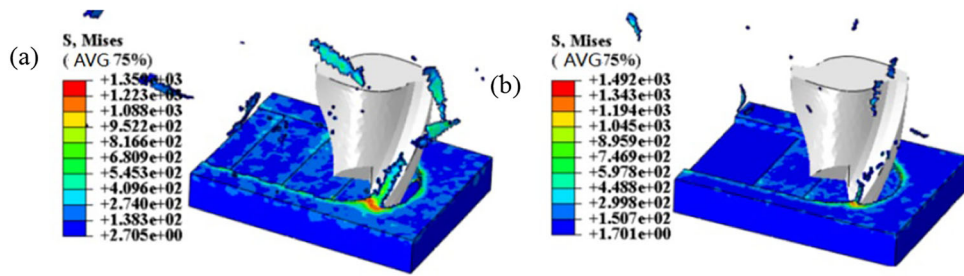
Fig. 3 Micro-milling simulation. (a) Conventional dry milling (b) Cryogenic cooling milling
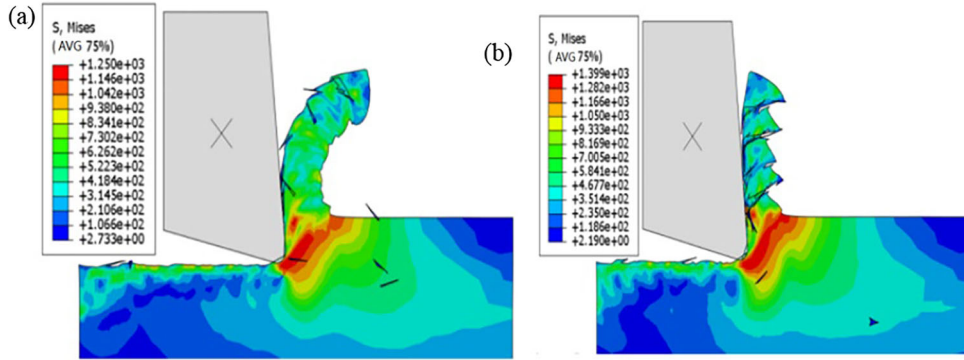

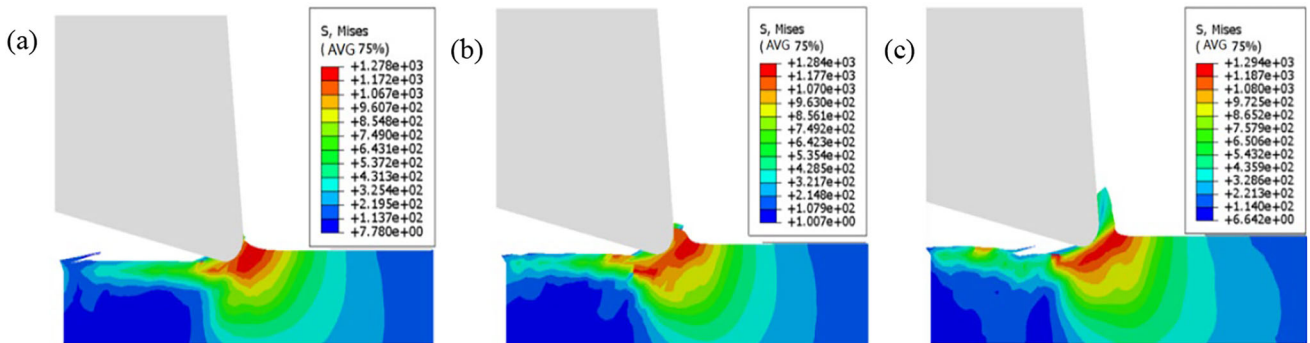**Fig. 4** Milling chip formation. (a) Conventional dry milling (b) Cryogenic cooling milling

Fig. 5 Cloud diagram of normal temperature micro-milling. (a) $h_D = 0.2r_\varepsilon$ (b) $h_D = 0.25r_\varepsilon$ (c) $h_D = 0.3r_\varepsilon$
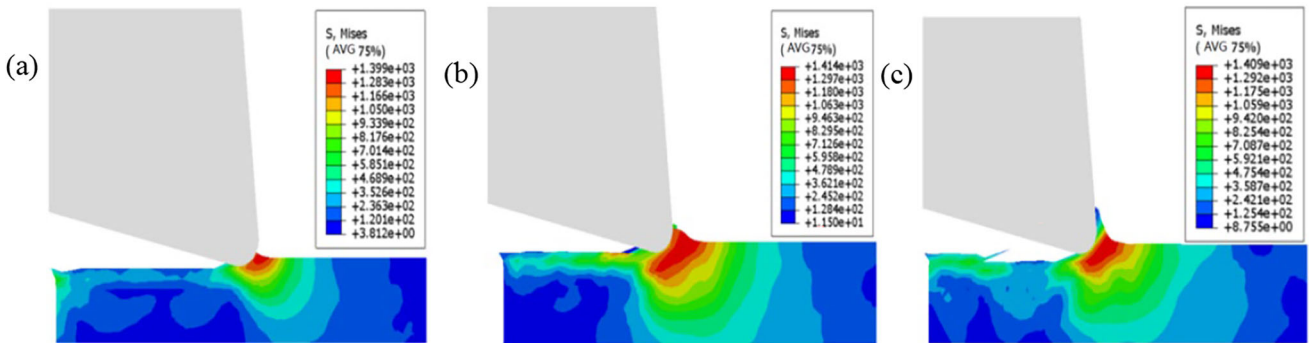

Fig. 6 Cloud diagram of cryogenic micro-milling. (a) $h_D = 0.2r_\varepsilon$ (b) $h_D = 0.25r_\varepsilon$ (c) $h_D = 0.3r_\varepsilon$

Through the simulation analysis of the minimum milling thickness, the appropriate tool can be selected in advance and the minimum depth of cut and feed per tooth can be carried out and avoid the micro-milling defects caused by scale effect.

3. Experimental Details

3.1 Experimental Material

The difficult-to-machining material Ti-6Al-4V alloy used in aerospace was investigated, and its elemental components are shown in Table 3. And then it was cut into 100 mm × 100 mm × 10 mm square piece by wire-electrode cutting machine. After that, the surface is clean.

3.2 Experimental Equipment

A self-assembled SL30 Micro high-precision CNC micro-milling platform was utilized for micro-milling experiments, its travel in $X/Y/Z$ direction was 250, 220, and 200 mm, the maximum clamping size was 200 × 200 mm, and the maximum spindle speed was 24,000 r/min, as shown in Fig. 7(a).

The cryogenic cooling milling experiment was carried out as shown in Fig. 7(b), and a three-phase dynamometer (Kisler9257B, Swiss) with 100 kHz data acquisition frequency was utilized to measure cutting force of cutting point. Meanwhile, the milling force was collected by a data collector (Fig. 7c).

Besides, as shown in Fig. 7(d), a C-CES 2010 integral micro-double-edge carbide tool with 5 μm tool edge radius (Fig. 7e) was adopted, and the tool parameters are shown in Table 4. Figure 7(f) expresses the LN_2 conveying device. In detail, the LN_2 tank was a self-pressurized DPL-175MP Dewar produced by Beijing Tianhai Company. Its pressure adjustment range was 0-1.4 MPa.

3.3 Experimental Scheme

The detailed milling parameters including conventional dry micro-milling and cryogenic are expressed in Table 5. Using single factor method, the micro-milling parameters were spindle speed of $n = 12000$ r/min, the cutting depth of $a_p = 20$, 30, 40, and 50 μm, the feed of $f_z = 1$, 1.5, 2, and 2.5 μm/r, and the milling groove width of $a_e = 1$ mm. Furthermore, the cryogenic temperature was controlled at -190 °C, as well as the conventional dry milling temperature 20 °C.

3.4 Analysis Equipment

An ultra-deep microscope digital microscope (KEYENCE VHX-1000, Japan) with magnification of 20-200 times was used to measure workpiece surface morphology. A SKF TKDT 10 contact thermometer was employed to measure the cooling temperature. Its temperature measurement range was -200 to 1200 °C with a resolution of 0.1 °C.

3.5 Temperature Measurements Experiment

A standard K-type thermocouple with 0.2 mm diameter and 0.2 s thermal response time was employed to measure the processing area temperatures. Meanwhile, the detected signal can be treated and expressed in a temperature measurement instrument. The milling temperature is illustrated in Fig. 8, the thermocouple was installed in a 0.3 mm diameter hole, and the hole was positioned on the machined surface.

4. Results and Discussion

4.1 Surface Morphology

Conventional micro-milling commonly leads to higher temperatures and increases more material plasticity, which results in significantly machined surface defects. As expressed in Fig. 9(a), adhesion, rupture, pitting damage and furrows defects are easily existed on the grooves surface.

Similarly, there are obviously a large number of micro-burrs in the grooves edge as shown in Fig. 9(b). These burrs will inescapably reduce the surface quality and dimensional accuracy, which seriously restricts the use of the machining parts. Furthermore, the chip appears as a long band (Fig. 9c), which can be seen that it is not easy to break chips during milling.

Through the strong cryogenic impact of LN_2, the plasticity of workpiece is significantly reduced, which effectively inhibits the ability of material plasticity deformation. The failure point in micro-milling groove, the particle adhesion and other defects are all reduced. Meanwhile, the feed trace obviously has shown more regular characteristics (Fig. 10a).

Compared to conventional milling, the cut of the processed groove is smooth, and the presence of burrs is hardly visible in Fig. 10(b). In addition, the chip is expressed the short strip (Fig. 10c), which means easy break chips.

Figure 11 expresses machining surface defects in conventional milling, there are a large number of continuous burrs on both sides of the groove, and the failure points inside the groove are more distributed as well as furrow scratches at lower feed.

As illuminated in Fig. 12, the machined surface at LN_2 cryogenic cooling is more complete. Although there are still trace fine burrs at the two dividing lines of the groove, the inner wall of machined surface is less damaged and the shape is smoother.

Cryogenic cooling impact can quickly penetrate into the contact friction surface between tool and chip, as well as the contact friction surface between tool and workpiece. It can effectively improve the processing environment of milling area and reduce the contact stress and friction. Besides, LN_2 can fully release a large number of generated milling heat, greatly reducing the milling temperature. The plasticity of workpiece surface is decreased, but brittleness is increased. For example, the tensile strength is increased from 960 MPa at flood 20 °C to 1500 MPa at cryogenic -196 °C, and the elastic modulus is also increased from 107 to 133 GPa (Table 1). Meanwhile, the tool adhesion effect will also be improved, as well as the hardness of tool and workpiece. Therefore, a processed surface

Table 3 Main elemental composition of Ti-6Al-4V, wt.%

Al	V	O	Fe	Others	Ti
5.5-6.75	3.5-4.5	0.2-0.3	≤ 0.5	< 0.3	Allowance
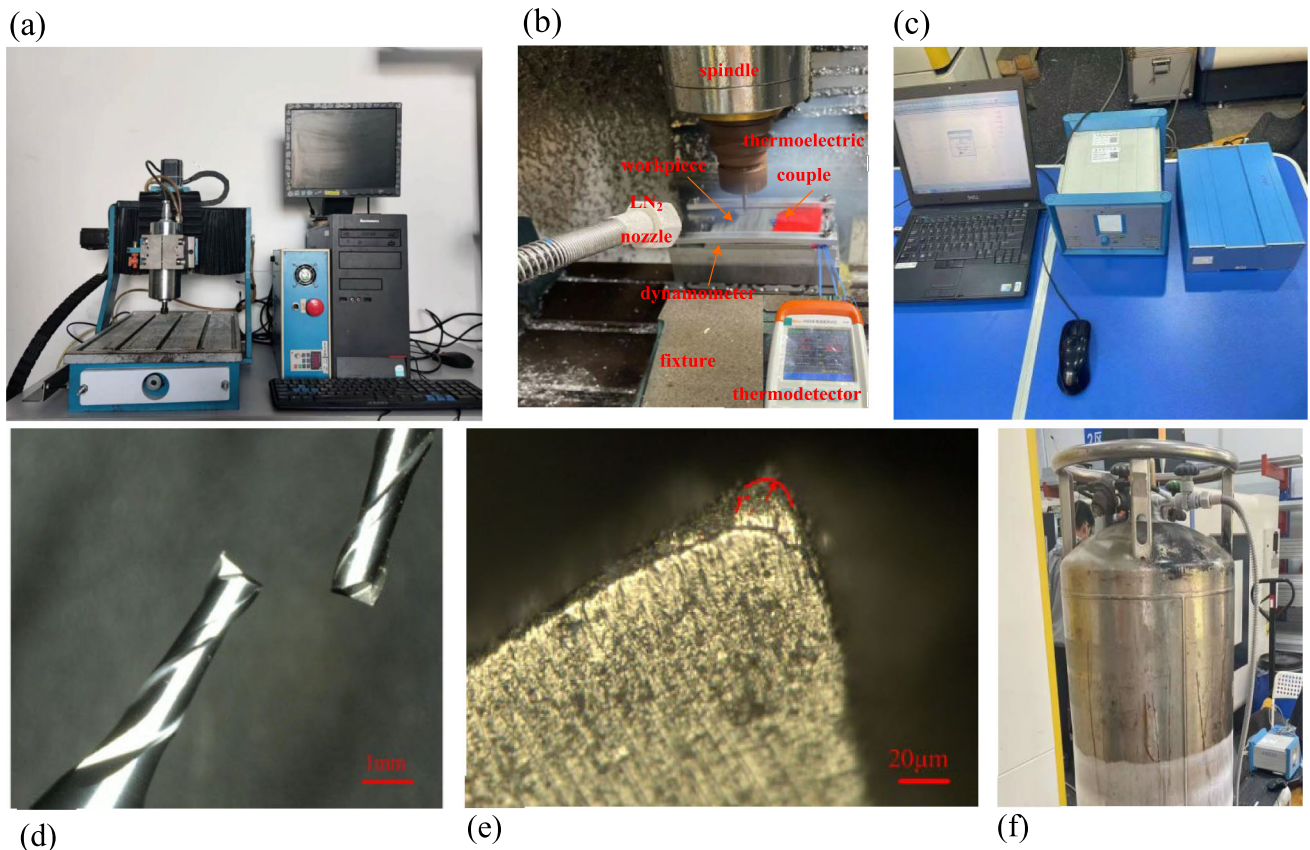
Fig. 7 Cryogenic experiment platform. (a) Micro-milling machine (b) Cryogenic milling (c) Milling force acquisition (d) Micro-tool (e) Tool nose (f) LN$_2$ tank

Table 4 Tool geometry parameter

Blade diameter, mm	Rake angle, °	clearance angle, °	Spiral angle, °	Edge radius, mm
1	6	12	30	0.005

Table 5 Milling parameters

Milling speed v_c, m/min	Depth of cut a_p, μm	Feed f_z, μm/r	Radial depth of cut a_e, mm	Cooling temperature T, °C
40	20	1		Dry milling 20
	30	1.5	1	
	40	2		
	50	2.5		LN$_2$ − 190

with smoother, less failure and clear feed marks can be obtained.

4.2 Surface Roughness

As can be seen from Fig. 13(a), with the continuous increase of feed per tooth, the surface roughness of workpiece under two kinds of milling strategies is first slowly decreased and then continuously increased. But the roughness value is lower under cryogenic cooling. When $f_z = 1$ μm/z, the material only generates elastic–plastic deformation, and the plowing and scratching are obviously through the tool action on workpiece. So, the surface quality is poor, and this research is similar to Ercetin (Ref 37) and Gandjar et al. (Ref 38). With the increase of feed, there began to be chip production, and the surface roughness value is decreased. When f_z is greater than 1.5 μm/z, the workpiece material is basically removed through shear action, and there increases material removal rate per unit time, which results in the increase of surface roughness value.

As shown in Fig. 13(b), the surface roughness of conventional micro-milling is increased with the increased depth of cut. The main reason is that the increase of depth of cut will improve the blade cutting burden and result in a corresponding increase for mill force, as well as cutting vibration. This leads to the machined surface ripple. Similarly, with the increase of depth of cut, the plastic deformation of the material will be

increased (Ref 39), which intensifies the friction contact between tool and workpiece, and the surface roughness will be increased.

The surface roughness after cryogenic cooling milling is significantly lower than that of conventional one. This research result is consistent with the results obtained by the non-micro-milling of titanium alloy (Ref 40). On the one hand, the toughness of titanium alloy is reduced at cryogenic cooling, the brittleness is increased, and the crack expansion is easy when the external force is impacted. So, the cutting fracture is smooth. On the other hand, cryogenic cooling can significantly reduce the milling temperature, and LN_2 jet can take away the chips in time and reduce the friction of tool and machining surface, which protects the tool and slows down the wear.
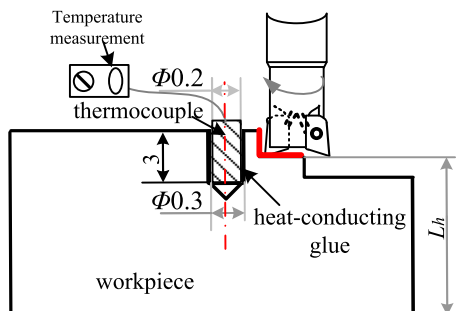
Fig. 8 Temperature measurement test

4.3 Milling Force

Compared to conventional milling, the milling force is bigger at cryogenic as illuminated in Fig. 14(a), which is beneficial for chip breaking. Meanwhile, in the range of 1-2.5 μm/z per tooth feed, the main milling force (radial force) decreases first and then increases. For the micro-tool with an edge radius of 5 μm, the milling feed of 1.5 μm is approximately the minimum milling thickness, and a scale effect is generated and the milling force is minimal. With the increasing of feed pre tool, the milling removal amount is increased, and the milling force is continuously risen under the action of chip extrusion. In the depth of cut range of 20-50 μm in Fig. 14(b), the main milling force is increased with the increase of the depth of cut. With the increase of the depth of cut, the removal thickness of material per unit time is significantly increased, the extrusion friction between the tool and machined surface is intensified, and the micro-milling force shows an upward tendency.

4.4 Milling Temperature

It can be seen from the literature (Ref 39) that the convective heat transfer coefficient of heat transfer medium could reflect the speed of heat transfer. Similarly, the convective heat transfer coefficient of water-miscible cutting fluids was 200-1000 W/(m^2 K), but 4000-6000 W/(m^2 K) for LN_2. As shown in Fig. 15(a), the temperature simulation analysis results show that the highest milling zone temperature is 242 °C. The milling temperature of tool shows a clear gradient, and the highest temperature is at the tool tip area. Meanwhile, the
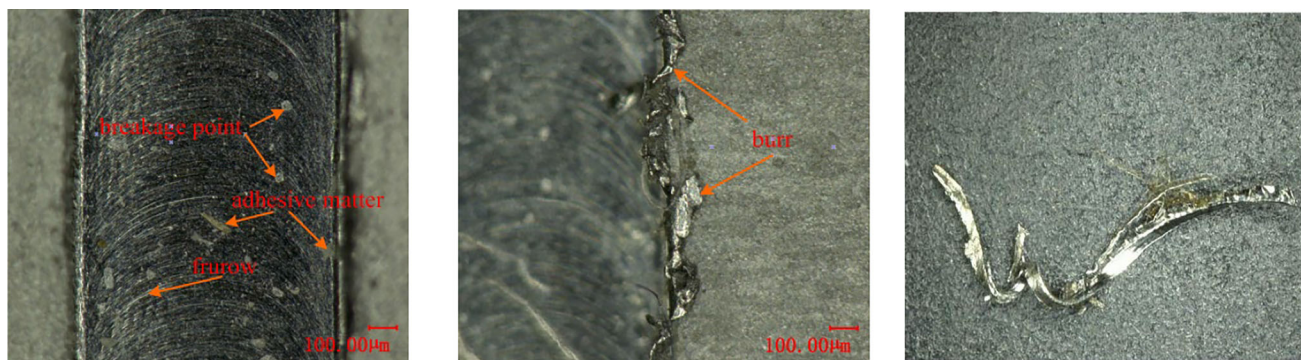

Fig. 9 Surface morphology of conventional milling (f_z = 2.5 μm/z, a_p = 20 μm). (a) Groove inner surface (b) Groove boundary (c) Chip shape
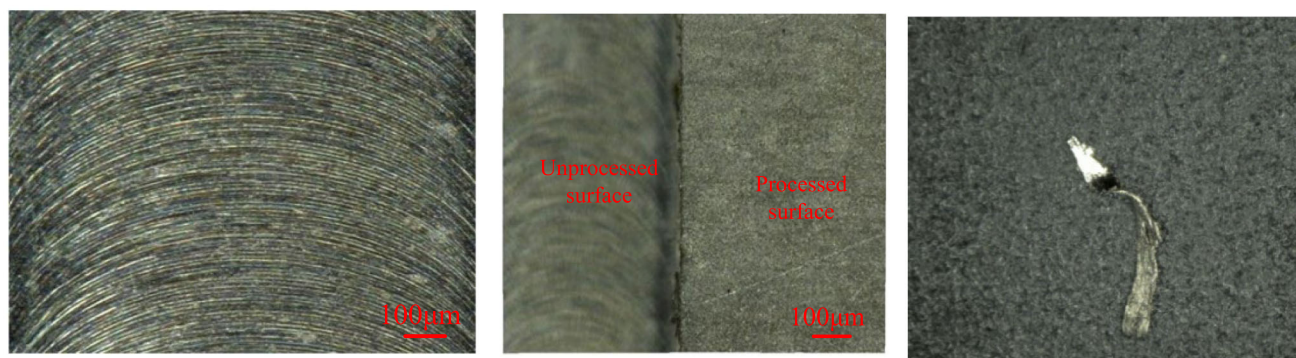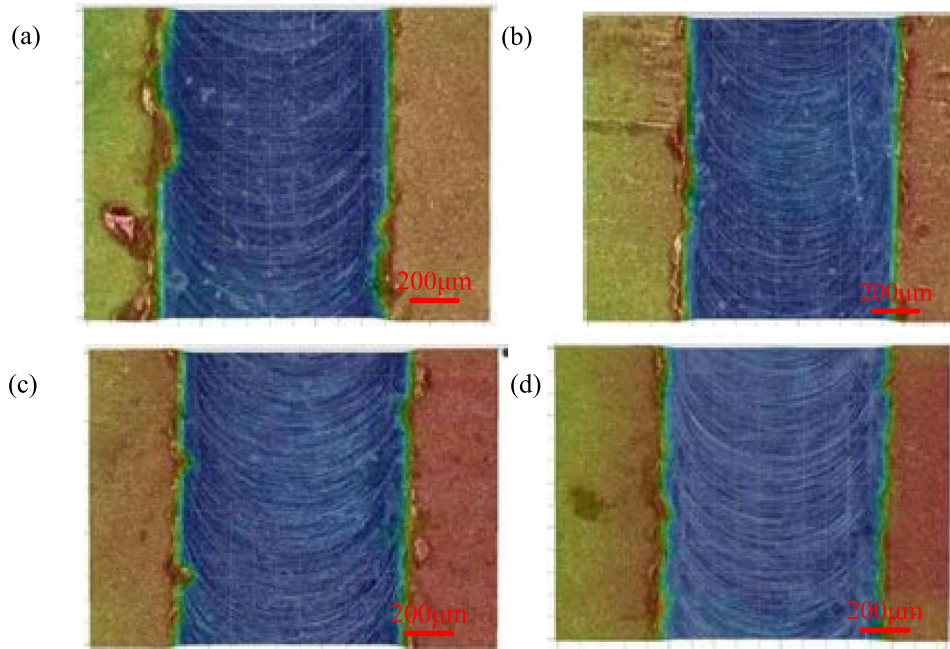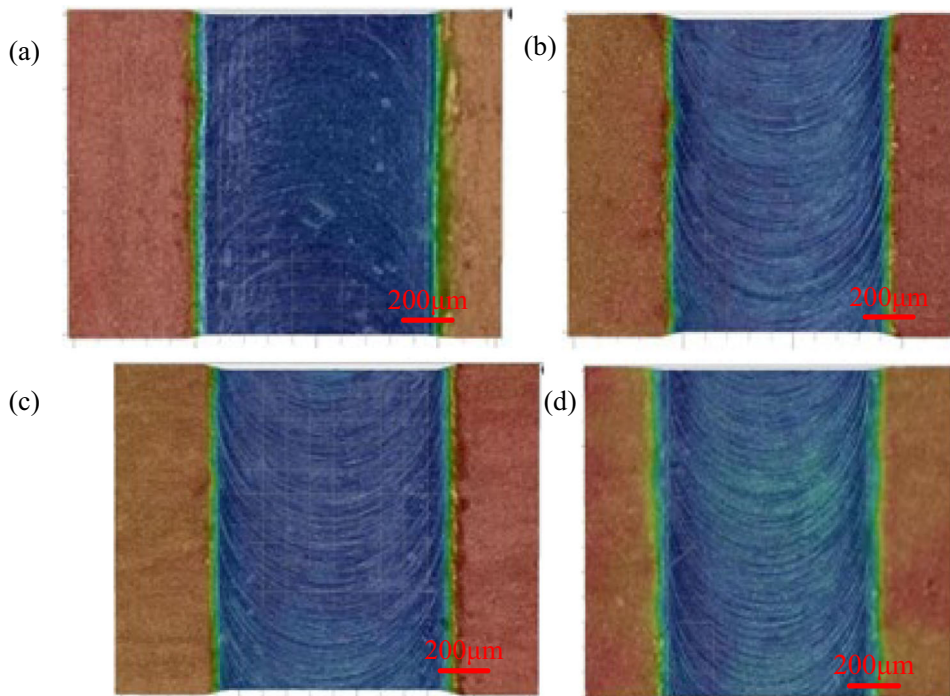

Fig. 10 Surface morphology of cryogenic cooling milling (f_z = 2.5 μm/z, a_p = 20 μm). (a) Groove inner surface (b) Groove boundary (c) Chip shape

Fig. 11 3D overall view of the processed surface under conventional milling. (a) $f_z = 2.5$ μm/z, $a_p = 50$ μm (b) $f_z = 2$ μm/z, $a_p = 40$ μm (c) $f_z = 1.5$ μm/z, $a_p = 30$ μm (d) $f_z = 1$ μm/z, $a_p = 20$ μm


Fig. 12 3D overview of processed surface under cryogenic cooling. (a) $f_z = 2.5$ μm/z, $a_p = 50$ μm (b) $f_z = 2$ μm/z, $a_p = 40$ μm (c) $f_z = 1.5$ μm/z, $a_p = 30$ μm (d) $f_z = 1$ μm/z, $a_p = 20$ μm

temperature of other parts decreases away from the cutting area. Through the temperature display of the tool and milling process, most of generated heat is taken away by the chips, and the part of heat is transferred to titanium workpiece and tool. It can be expressed in Fig. 15(b) that the highest milling temperature at cryogenic cooling is lower than 105 °C and concentrated at the tool nose. It can deduce that LN$_2$ can significantly reduce the milling temperature compared to conventional micro-milling.
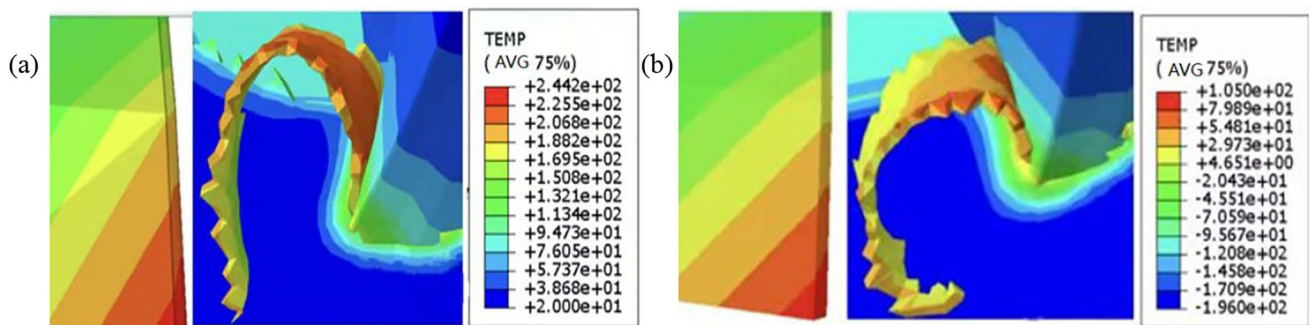
In conventional milling (Fig. 16a), milling temperature is increased with the increase of feed per tooth, but the overall increase is not obvious, and the temperature can be reached more than 170 °C. But the cryogenic cooling can greatly reduce milling temperature which is less than 45 °C, and the increasing tendency is small with the increase of feed per
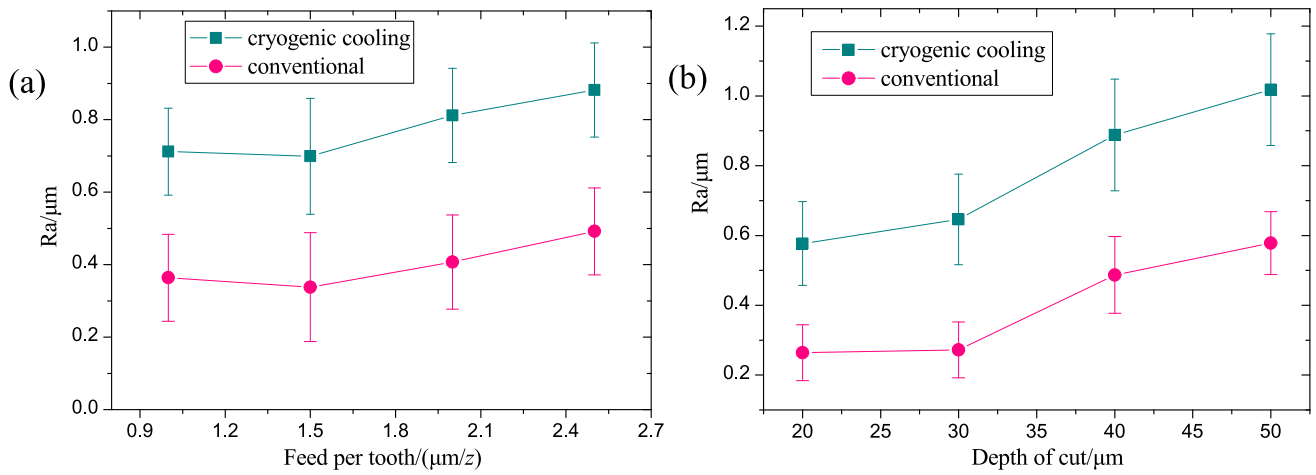
Fig. 13 Effect of milling parameters on surface roughness. (a) Feed per tooth (b) Depth of cut
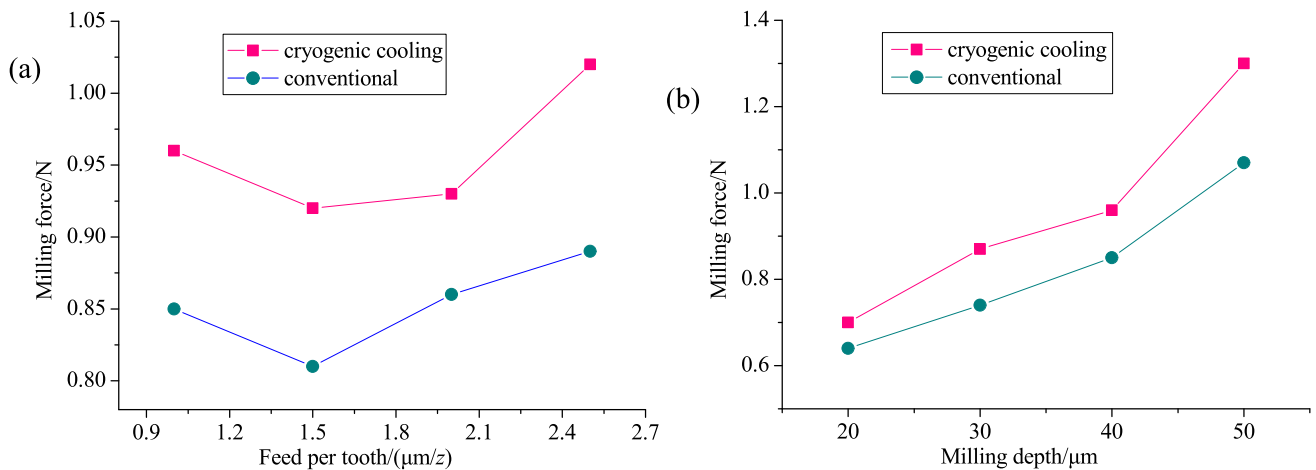
Fig. 14 Effect of milling parameters on milling force. (a) Feed per tooth (b) Depth of cut

Fig. 15 Milling temperature simulation. (a) Conventional dry micro-milling (b) Cryogenic cooling micro-milling

tooth. In detail, when $f_z < 1.5 \ \mu m/z$, the temperature has an obvious increasing tendency. After $f_z > 1.5 \ \mu m/z$, the increasing trend is more gentle. Therefore, a larger per tooth feed can be optimization at LN_2 cryogenic cooling, which can not only ensure low milling temperature but also improve processing efficiency.

As expressed in Fig. 16(b), the milling temperature is proportional to depth of cut for conventional milling, as well as a trend of increasing. When depth of cut is increased from 20 to 50 μm, the milling temperature is improved from 140 to 180

with 40 °C temperature rise deviation. At cryogenic, LN_2 can quickly absorb cutting heat and dissipate quickly, which results in the lower overall milling temperature. It can be seen that the depth of cut is the most important factor affecting on the milling temperature. So, the cutting depth should be kept smaller at cryogenic cooling micro-milling titanium alloy.

4.5 Tool Wear

When the same processing parameter, the tool wear under conventional dry micro-milling is more serious (Fig. 17a), the
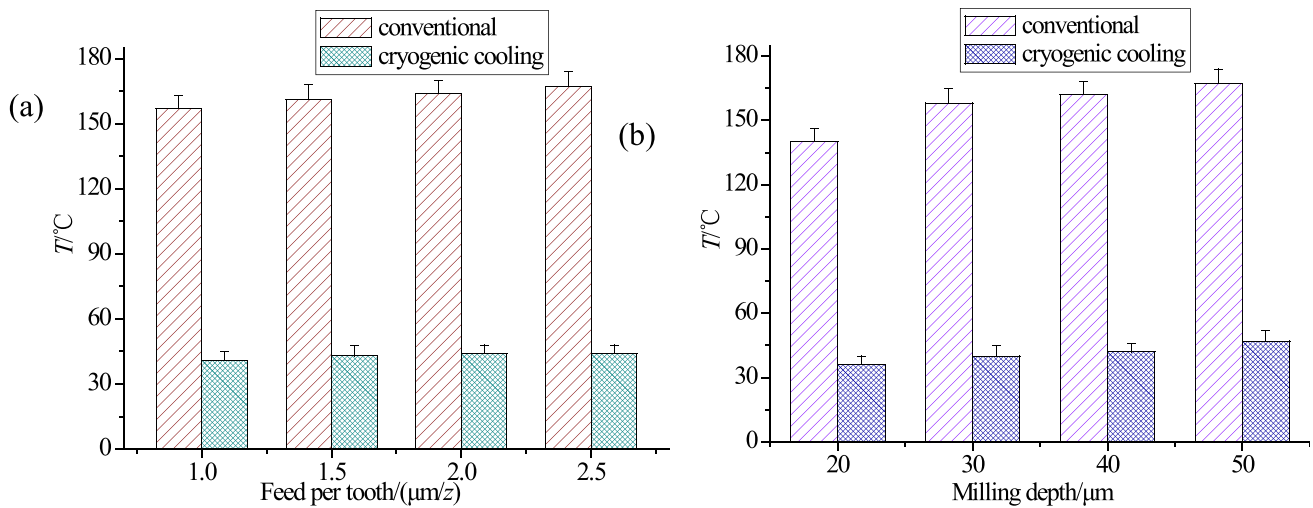
Fig. 16 Effect of milling parameters on milling temperature. (a) Feed per tooth (b) Depth of cut
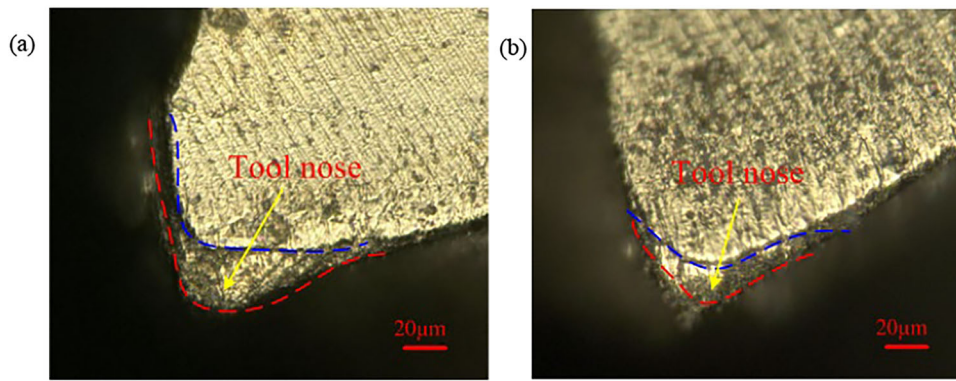
Fig. 17 Milling temperature simulation. (a) Conventional dry micro-milling (b) Cryogenic cooling micro-milling

wear amount at tool nose cutting area is obviously more than 40 μm, and the wear is very serious. On the contrary, under cryogenic cooling condition, the wear at tool nose is less than 20 μm (Fig. 17b), and the tool is still in the normal steady working phase stage. It can be revealed that cryogenic cooling significantly improves the life of micro-milling tool. It has the same results with the non-micro-milling process (Ref 40, 41).

5. Conclusions

Based on the methodology applied on the present study, the following conclusions can be claimed.

1. The minimum milling thickness model is established considering scale effect, and the minimum milling thickness is simulated and deduced. When the milling thickness is $0.2r_\varepsilon$, there are no chips. When it continues to be increased to $0.25r_\varepsilon$, the workpiece begins to express the elastic–plastic deformation. When the milling thickness increases to $0.3r_\varepsilon$, the chips are generated.
2. Compared to conventional milling, the processed groove is smooth, and the presence of burrs is hardly visible at cryogenic cooling, and that can also easily generate chips breaking. Furthermore, the surface roughness value is obviously decreased.
3. Compared to conventional milling, the milling force is bigger at cryogenic cooling which is beneficial for chip breaking. Because of the scale effect, the main milling force decreases first and then increases in the range of f_z = 1-2.5 μm/z. A scale effect can be expressed at $f_z <$ 1.5 μm, and at f_z = 1.5 μm it has the smallest milling force.
4. For LN$_2$ cryogenic cooling micro-milling titanium alloy, a larger per tooth feed and lower depth of cut can be optimized, which can not only ensure machining properties as well as tool life but also improve processing efficiency as a result of cryogenic.

The micro-milling titanium alloy process is widely used in industrial manufacture, and the machining properties can be significantly improved at cryogenic cooling. So, the research results can provide reference in similar micro-machining production.

References

1. B.F. Wang, J. Li, and J.Y. Sun, Adiabatic Shear Bands in Ti-6Al-4V Alloy with Lamellar Microstructure, *J. Mater. Eng. Perform.*, 2014, **23**(5), p 1896–1903
2. S. Alborz, D. Vimal, and T.N. Stephen, Investigation of the Effects of Cryogenic Machining on Surface Integrity in CNC End Milling of Ti-6Al-4V Titanium Alloy, *J. Manuf. Process.*, 2016, **21**, p 172–179
3. S. Sun, M. Brandt, and S. Palanisamy, Effect of Cryogenic Compressed Air on the Evolution of Cutting Force and Tool Wear during Machining of Ti–6Al–4V Alloy, *J. Mater. Process. Technol.*, 2015, **221**, p 243–254
4. G. Kibria, B.R. Sarkar, and B.B. Pradhan, Comparative Study of Different Dielectrics for Micro-EDM Performance during Microhole Machining of Ti-6Al-4V Alloy, *Int. J. Adv. Manuf. Technol.*, 2010, **48**(5–8), p 557–570
5. T. Schaller, L. Bohn, and J. Mayer, Microstructure Grooves with a Width of Less Than 50 μm Cut with Ground Hard Metal Micro End Mills, *Precis. Eng.*, 1999, **23**(10), p 229–235
6. C. Nath, S.G. Kapoor, A.K. Srivastava, and J. Iverson, Study of Droplet Spray Behavior of an Atomization-Based Cutting Fluid Spray System for Machining Titanium Alloys, *J. Manuf. Sci. Eng.*, 2014, **136**(2), p 1004–1012
7. K. Aslantas, M. Danish, A. Hasçelik, M. Mia, M. Gupta, T. Ginta, and H. Ijaz, Investigations on Surface Roughness and Tool Wear Characteristics in Micro-turning of Ti-6Al-4V Alloy, *Materials*, 2020, **13**(13), p 2998
8. B.G. Martin, X.Y. Liu, and E.D. Richard, Investigation of the Dynamics of Micro End Milling Part I: Model Development, *J. Manuf. Sci. Eng.*, 2006, **128**, p 893–900
9. W.Y. Bao and I.N. Tansel, Modeling Micro-end-milling Operations. Part II: Tool Run-Out, *Int. J. Mach. Tools Manuf*, 2000, **40**, p 2175–2192
10. X. Liu, R.E. DeVor, and S.G. Kapoor, The Mechanics of Machining at the Micro Scale: Assessment of the Current State of the Science, *J. Manuf. Sci. Eng.*, 2004, **126**(4), p 666–678
11. K. Lee and D.A. Dornfeld, An Experimental Study on Burr Formation in Micro Milling Aluminum and Copper, *Trans. NAMRI/SME*, 2002, **30**, p 1–8
12. J. Schmidt and H. Tritschler, Micro Cutting of Steel, *Microsyst. Technol.*, 2004, **10**(3), p 167–174
13. T.J. Fu, *Research on Burr Formation and Control Technology in Micro-milling*. Dissertation: Shandong University (2014)
14. S. Subbiah, *Some Investigations of Scaling Effects in Micro-cutting*. Dissertation: Georgia Institute of Technology (2006)
15. E.M. Kopalinsky and P.L.B. Oxley, Size Effects in Metal Removal Processes, *Inst. Phys. Conf. Ser.*, 1984, **70**, p 389–396
16. M. Mozammel, Multi-response Optimization of End Milling Parameters under through-Tool Cryogenic Cooling Condition, *Measurement*, 2017, **111**, p 134–145
17. K.H. Park, M.A. Suhaimi, and G.D. Yang, Milling of Titanium Alloy with Cryogenic Cooling and Minimum Quantity Lubrication (MQL), *Int. J. Precis. Eng. Manuf.*, 2017, **18**(1), p 5–14
18. A. Shokrani, V. Dhokia, and S.T. Newman, Comparative Investigation on Using Cryogenic Machining in CNC Milling of Ti-6Al-4V Titanium Alloy, *Mach. Sci. Technol.*, 2016, **20**(3), p 475–494
19. Y. Kakinuma, N. Yasuda, and T. Aoyama, Micro Machining of Soft Polymer Material Applying Cryogenic Cooling, in *Proceedings of International Conference on Leading Edge Manufacturing in 21st century 4: 9A135* (2007)
20. K. Aslantas, A. Hasçelik, A. Erçetin, M. Danish, K.H. Alatrushi Luqman, S. Rubaiee, and A.B. Mahfouz, Effect of Cutting Conditions on Tool Wear and Wear Mechanism in Micro-milling of Additively Manufactured Titanium Alloy, *Tribol. Int.*, 2024, **193**, 109340
21. M. Perçin, K. Aslantas, İ Ucun, Y. Kaynak, and A. Çicek, Micro-drilling of Ti-6Al-4V Alloy: The Effects of Cooling/Lubricating, *Precis. Eng.*, 2016, **45**, p 450–462
22. İ Ucun, K. Aslants, and F. Bedir, The Effect of Minimum Quantity Lubrication and Cryogenic Pre-cooling on Cutting Performance in the Micro Milling of Inconel 718, *Proc. Inst. Mech. Eng. Part B J. Eng. Manuf.*, 2014, **229**, p 2134–2143
23. G.R. Johnson and W.H. Cook, A Constitutive Model and Data for Metals Subjected to Large Strains, High Strain Rates and High Temperatures, *ASME J. Eng. Mater. Technol.*, 1983, **102**(4), p 541–547
24. L.Y. Zhou, R.C. Wang, and X.F. Wang, Thermal Deformation Behavior and Constitutive Model of SiCp/2014Al Composite Materials, *Nonferr. Met. Sci. Eng.*, 2021, **12**(4), p 66–74
25. G.I. Taylor, The Use of Flat-Ended Projectiles for Determining Dynamic Yield Stress. I: Theoretical Considerations, *Proc. R. Soc. Lond. A*, 1948, **194**, p 289–299
26. S.S. Joshi and S.N. Melkote, An Explanation for the Size-Effect in Machining Based on Strain Gradient Plasticity, *J. Manuf. Sci. Eng. Trans. ASME*, 2004, **126**(4), p 679–684
27. M. Asad, T. Mabrouki, and F. Girardin, Towards a Physical Comprehension of Material Strengthening Factors during Macro to Micro-scale Milling, *Mechanics*, 2011, **17**(1), p 97–104
28. D.A. Lucca, Y.W. Seo, and R. Komanduri, Effect of Tool Edge Geometry on Energy Dissipation in Ultraprecision Machining, *Ann. CIRP*, 1993, **42**(1), p 83–86
29. M.S. Seong, S.L. Han, and H.A. Jung, Effects of the Friction Coefficient on the Minimum Cutting Thickness in Micro Cutting, *Int. J. Mach. Tools Manuf*, 2005, **45**, p 529–535
30. J. Jiang, Y.Q. Li, and Z.Y. Zhang, *Manufacturing Technology of Titanium Alloy Parts*, National Defence Industry Press, Beijing, 1991
31. Q. Xu, *A Design of Cooling System and Cutting Experiments for the Cryogenic Machining of Difficult-to-Cut Materials*. Dissertation: Nanjing University of Aeronautics and Astronautics (2018)
32. J.Y. Wang and Z.M. Ge, *Aviation Titanium Alloy*, Shanghai Science and Technology Press, Shanghai, 1985
33. J.H. Zuo, *Environmental Effects on the Mechanical Performance of Ti-6Al-4V Alloy*. Dissertation: Institute of metals Research, Chinese Academy of Sciences (2008)
34. J.W. Zhu, X.B. Lei, and T. Zhang, Model and Analysis of Mesoscopic Minimum Cutting Thickness, *Mech. Strength*, 2022, **44**(04), p 930–936
35. D. Majcherczak, P. Dufrenoy, and Y. Berthier, Tribological, Thermal and Mechanical Coupling Aspects of the Dry Sliding Contact, *Tribol. Int.*, 2007, **40**(5), p 834–843
36. Z.L. Gong and P. Huang, Calculating Model and Corresponding Analysis of Sliding Friction Coefficient Based on Thermal Dynamic Coupling, *J. South China Univ. Technol.*, 2008, **36**(4), p 10–13
37. A. Ercetin, K. Aslantaş, Ö. Özgün, M. Perçin, M. Patel, and G. Chandrashekarappa, Optimization of Machining Parameters to Minimize Cutting Forces and Surface Roughness in Micro-milling of Mg13Sn Alloy, *Micromachines*, 2023, **14**(8), p 1590
38. K. Gandjar, M. Adrian, A. Maulana, and K.T. Jo, The Effects of Cutting Parameters to the Surface Roughness in High Speed Cutting of Micro-milling Titanium Alloy Ti-6Al-4V, *Key Eng. Mater.*, 2020, **5969**, p 133–138
39. F. BarrnR and G.F. Nellis, *Cryogenic Heat Transfer*, CRC Press, Raton, 2016
40. F.B. Wang and Y.Q. Wang, Investigate on Effect of Cryogenic Cooling on Oxidation Wear of WC-Co Carbide Tool Milling Titanium Alloy, *Mach. Sci. Technol.*, 2019, **23**(6), p 906–924
41. F.B. Wang and Y.Q. Wang, Cleaner Milling on Ti-6Al-4V Alloy Cooled by Liquid Nitrogen: External Spray and Inner Injection, *Int. J. Adv. Manuf. Technol.*, 2021, **112**(3), p 1193–1206